https://doi.org/10.15623/ijret.2018.0709004 Received: 16-06-2018, Accepted: 28-07-2018, Published: 18-08-2018

SYNTHESIS AND THE STUDY OF PHOTOCATALYTIC ACTIVITY OF COBALT FERRITE ($COFE_2O_4$) NANOPARTICLES: SYNERGISTIC EFFECTS OF PHOTOCATALYSIS AND PHOTO-FENTON PROCESS

Srinivas. M[1], L.Gomathi Devi[2]

[1]*Department of Post Graduate Studies in Chemistry, Central College City Campus, Dr. Ambedkar Street, Bangalore University, Bangalore-560001, India*

[2]*Department of Post Graduate Studies in Chemistry, Central College City Campus, Dr. Ambedkar Street, Bangalore University, Bangalore-560001, India*

Abstract

$CoFe_2O_4$ was prepared by sol-gel combustion method. Powder X-ray diffraction (PXRD) studies confirmed the spinel structure for $CoFe_2O_4$. UV-Vis absorbance spectrum and the following Kubelka-Munk plot show the band gap of $CoFe_2O_4$ to be 2.73eV. FTIR studies shows the existence of Co-O and Fe-O stretching vibrations. Raman spectroscopy gives the information pertaining to tetrahedral and octahedral sites. The activity of the catalyst was explored for the degradation of methyl orange in presence of peroxymonosulphate (PMS) as an oxidant which is dipolar, possessing unsymmetrical structure and higher oxidation potential and shows better oxidising reactions due to charge transfer to solvent molecule (CTTS) and PMS forms a charge transfer complex with $CoFe_2O_4$. The active roles of the hydroxyl and sulphate free radicals are confirmed. $CoFe_2O_4$ catalyst shows synergistic effect between photocatalysis and photo- Fenton process especially even at higher pH values and the catalyst is found to be stable and can be reused for three consecutive cycles.

Keywords: *Cobalt ferrite, peroxymonosulphate, photocatalysis, photo- Fenton process*

----------***----------

1. INTRODUCTION

The process of semiconductor photocatalysis has been widely used for the treatment of polluted water. There have been many reports in the literature dealing with the degradation of various organic pollutants through photocatalysis using metal oxide semiconductors under ultraviolet light irradiation [1-3]. Ferrites are viable alternative materials to TiO_2 to be used as photocatalysts for the hydrogen production and environmental remediation. Transition metal ferrites can be more appropriate and promising due to the several advantages like, it is an effective catalyst with specific active sites and most importantly its narrow band gap matches with the solar spectrum. Among the various semiconducting ferrite materials $CoFe_2O_4$ with spinel structure is more promising due to its narrow band gap, good photochemical stability, favourable magnetic property and it can exhibit characteristic photochemical reactions especially under the visible-light irradiation [4-6]. Spinels with only divalent ions in the tetrahedral sites are called normal spinels, while compounds with the presence of divalent ions in both the tetrahedral and octahedral sites are called inverse spinels. In the inverse spinel structure, all the Co^{2+} ions occupy the octahedral sites of lattice structure, half of the Fe^{3+} ions can also occupy the octahedral sites and the rest of the Fe^{3+} ions remain in the tetrahedral sites [7]. The ferrite spinel structure is based on cubic closed-packed oxygen lattice, in which tetrahedral (A sites) and octahedral (B sites) interstices are occupied by the cations. The selection of $CoFe_2O_4$ among other ferrites is based on its redox activity and especially its ability to store oxygen in the crystal lattice. Therefore, $CoFe_2O_4$ is an excellent candidate for the production of hydrogen from water under solar light illumination and also to degrade environmentally hazardous pollutants. It is well known that bivalent Co^{2+} and trivalent Fe^{3+} cations are distributed among the tetrahedral and octahedral sites and this special type of cationic distribution enhances the magnetic properties of spinel $CoFe_2O_4$ [8-10]. The presence of magnetic $CoFe_2O_4$ nanoparticles in a photocatalytic reaction system has an added advantage since these nanoparticles can be separated magnetically from the reaction solution and can be reused after appropriate treatment [11-16]. This research article deals with synthesis of $CoFe_2O_4$ by sol-gel combustion method and to probe its photocatalytic activity under visible light irradiation. The degradation reaction was further studied with an additional oxidant like peroxymonosulphate (PMS). To confirm the active role of free hydroxyl radicals, the reaction was also studied in the presence of methanol which acts as holes scavenger thereby indirectly predicts the active role of free hydroxyl radicals.

https://doi.org/10.15623/ijret.2018.0709004 Received: 16-06-2018, Accepted: 28-07-2018, Published: 18-08-2018

2. EXPERIMENTAL

2.1 Materials

Methyl Orange (MO) dye was obtained from Sigma Aldrich. Iron nitrate $Fe(NO_3)_2 \cdot 9H_2O$, cobalt nitrate $Co(NO_3)_2.6H_2O$ and methanol were obtained from Nice chemicals.

2.2 Synthesis of $CoFe_2O_4$ by Sol Gel Combustion Method

The procedure adopted in the present research work is similar to the method adopted by James wang et al.,[17]. $CoFe_2O_4$ was synthesized by sol-gel combustion method using $Fe(NO)_3 \cdot 9H_2O$, $Co(NO)_3 9H_2O$ and citric acid ($C_6H_8O_7 \cdot H_2O$). Citric acid (5% w/v) was first dissolved in distilled water to form a clear solution. Then stoichiometric amount of cobalt and ferric nitrates in the ratio of 1:2 were dissolved in the citric acid solution. The prepared solution was evaporated by continuous stirring and heating for 4 hours at 70 °C until it turns into a solid gel. Finally, the product was calcined in a furnace for 2 hours at 800 °C to obtain $CoFe_2O_4$.

2.3 Catalyst Characterization

The catalyst is characterized by the following techniques: powder X-ray diffraction (PXRD), Fourier transform infra red (FTIR) spectroscopic technique, UV-Vis absorption spectroscopic technique, Scanning Electron Microscope (SEM) equipped with Energy-Dispersive X-ray analysis (EDX), surface area measurements by Brunner–Emmet–Teller (BET) technique and X-ray photoelectron spectroscopy (XPS) techniques. The detail of the experiment and instrumentation is given elsewhere [18].

2.4 Photochemical Reactor

The detail pertaining to photocatalytic degradation experiments are given elsewhere [18].

3. RESULT AND DISCUSSION

3.1 PXRD Studies

PXRD pattern of $CoFe_2O_4$ shows peaks at different 2Θ values, which are represented along with respective hkl values as: 18.35º(111), 30.15º (220), 35.35º (311), 37.42º (222), 43.33º (400), 54.97º (422), 57.36º (511), 62.93º (440) 71.41º (622) 74.53º (533) (Figure 1) and it is in accordance with spinel structure with space group Fd3m which is in agreement with JCPDS standard card (22-1086). The crystallite size of $CoFe_2O_4$ was calculated by using the Scherrer's equation $D=K \lambda / \beta \cos \theta$. Where, λ is the wavelength, β is full width at half maximum diffraction plane, k is a shape factor and θ is angle of diffraction and the crystallite size was found to be 50.52 nm.

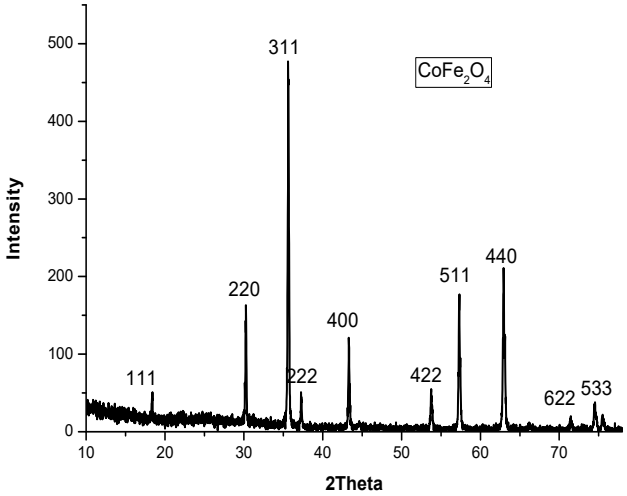

Fig 1: PXRD pattern of $CoFe_2O_4$

3.2 UV-Visible Absorption Spectroscopy

UV-Visible absorption spectrum of $CoFe_2O_4$ exhibits wide absorbance from UV to visible light region (Figure 2). The band gap values were determined from this spectrum by converting the absolute absorption values to Kubelka-Munk function of F (R∞). The plot of Kubelka-Munk function $[F(R\infty)hv]^{1/2}$ versus photon energy in electron volts (eV) gives the band gap energy value of $CoFe_2O_4$ as shown in the inset of Figure. 2. The energy band gap value of $CoFe_2O_4$ was found to be 2.73 eV**.** The transition metal ions having d-electrons show d-d transitions between t_2g to eg (Oh)/eg to t_2g (td) and these transitions are responsible in extending the absorption of the catalyst to the visible region. Electronic configuration of Co^{2+} having three unpaired d-electrons are involved in the d-d transitions, whereas Fe^{3+} is present in the stable half filled electronic configuration.

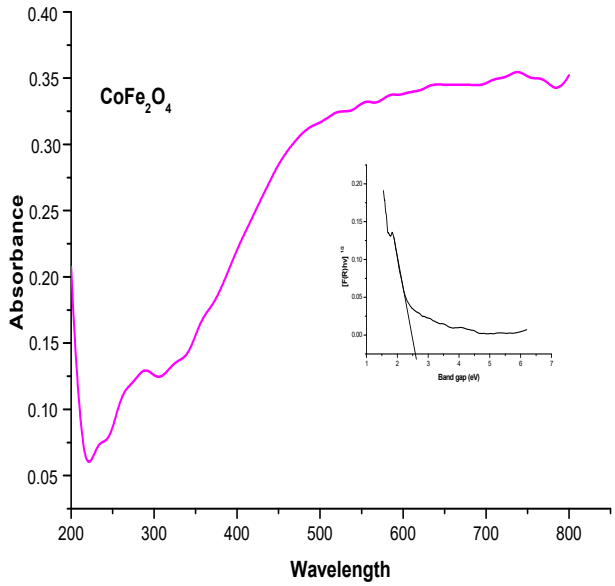

Fig 2: UV-visible absorbance spectrum of $CoFe_2O_4$ and Kubelka-Munk plot is shown in the inset.

https://doi.org/10.15623/ijret.2018.0709004 Received: 16-06-2018, Accepted: 28-07-2018, Published: 18-08-2018

3.3 FTIR

FTIR spectrum of $CoFe_2O_4$ shows two peaks, one at 557 cm^{-1} corresponding to the intrinsic stretching vibrations of Co-O and a small peak at 402 cm^{-1} belonging to Fe-O (Figure3).

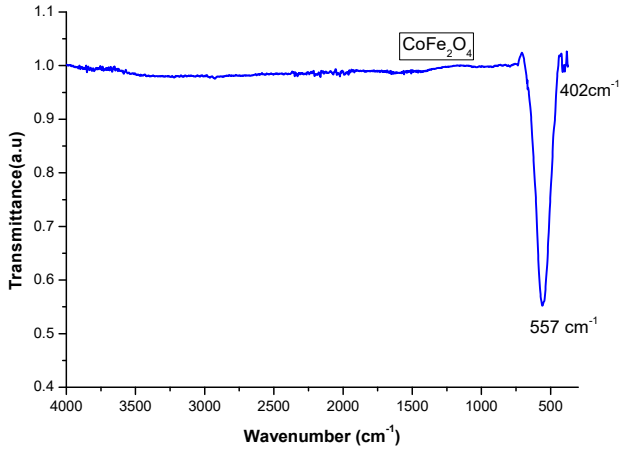

Fig 3: FTIR spectrum of $CoFe_2O_4$

3.4 FESEM

FESEM image of $CoFe_2O_4$ sample shows aggregation of spheres of almost uniform size and is as shown in the Figure 4a. The elemental composition of $CoFe_2O_4$ is given in the EDX spectrum (Figure 4b). The elemental composition of Fe and Co is found to be in the ratio of 2:1 as confirmed by the EDX technique.

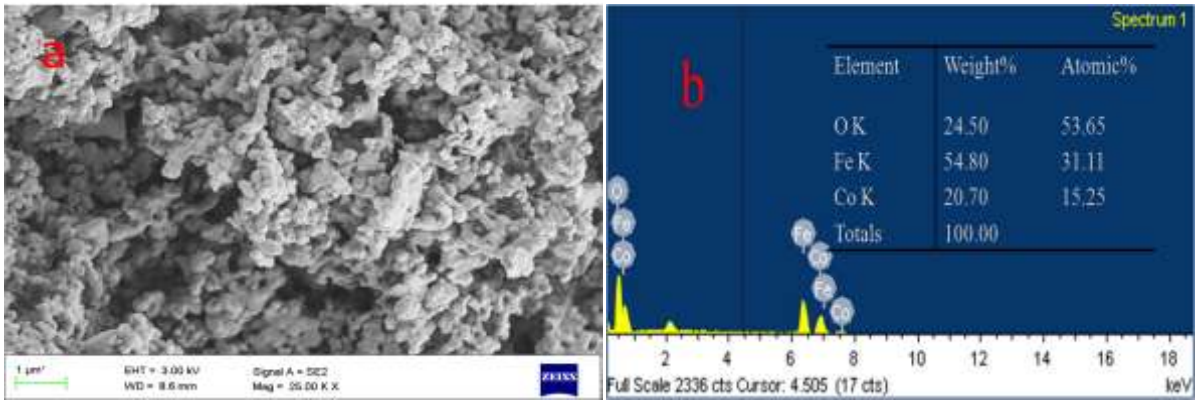

Fig 4: a FESEM image of $CoFe_2O_4$ and b EDS of $CoFe_2O_4$

3.5 Raman Spectroscopy

Figure 5.The Raman spectrum of $CoFe_2O_4$ shows peaks at 288 cm^{-1} (E_g) and 477 cm^{-1} (F_{2g}) and it is due to the phonon modes of metal ions involved in the octahedral groups. These modes correspond to symmetric and antisymmetric bending modes of oxygen atom in metal-oxygen bond at octahedral sites. The band at 700 cm^{-1} is of A_{1g} arises due to the motions of oxygen atoms in tetrahedral group [19-20].

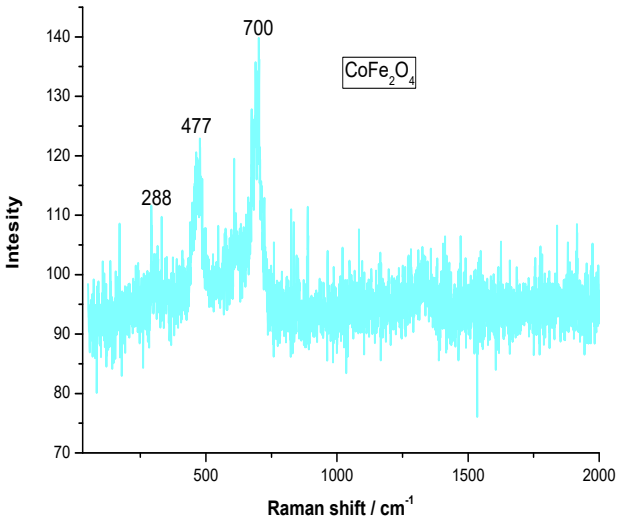

Fig 5: Raman spectrum of $CoFe_2O_4$

https://doi.org/10.15623/ijret.2018.0709004 Received: 16-06-2018, Accepted: 28-07-2018, Published: 18-08-2018

3.6 BET

The specific surface area and pore volume of $CoFe_2O_4$ sample was determined by BET method. The adsorption and desorption isotherms are shown in the Figure. 6 and the inset shows BJH pore size distribution curve. The pore size distribution was found to be the 1.3-6 nm. The specific surface area and the total pore volume were found to be 6.202 $m^2\ g^{-1}$ and 0.0031ccg^{-1} respectively.

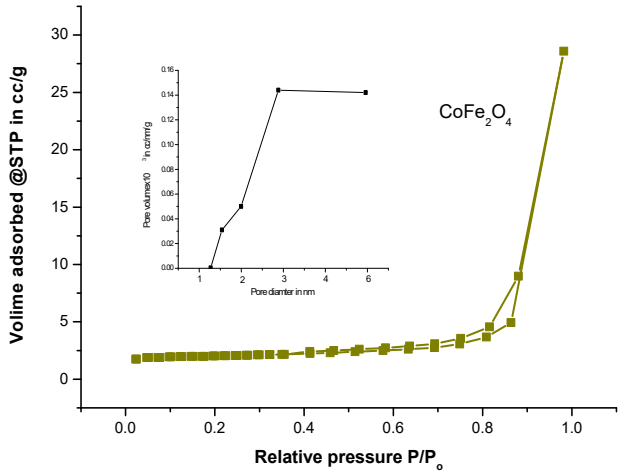

Fig 6: N_2 adsorption–desorption isotherm of $CoFe_2O_4$. BJH pore size distribution curve is represented in the Figure inset.

3.7 XPS

XPS spectrum of $CoFe_2O_4$ shows two Co^{2+} major peaks with binding energy (BE) values of 795.79 and 780.95 eV, corresponding to the $Co2p_{1/2}$ and $Co2p_{3/2}$ spin-orbit peaks respectively. The $Fe2p_{3/2}$ and $Fe2p_{1/2}$ states were observed at BE values of 710.89 and 724.72 eV. The peak in the range of 710-711eV is usually attributed to the Fe^{3+} cation located at the octahedral site in the spinal structure and the peak at 724.72 eV is endorsed to the Fe^{2+} cation located at the tetrahedral site in the spinal structure. In addition to the above peaks, two satellite peaks are observed at 786 and 719 eV corresponding to the $Co2p_{3/2}$ and $Fe2p_{3/2}$ respectively. The O1s BE peaks are observed at 530.95 and 532.04 eV. The BE peak at 530.95 eV can be assigned to the lattice-oxygen and the peak at 532.04 eV can be due to the OH species adsorbed on the surface of the $CoFe_2O_4$ sample. OH species is usually adsorbed at oxygen-deficient sites (Figure 7).

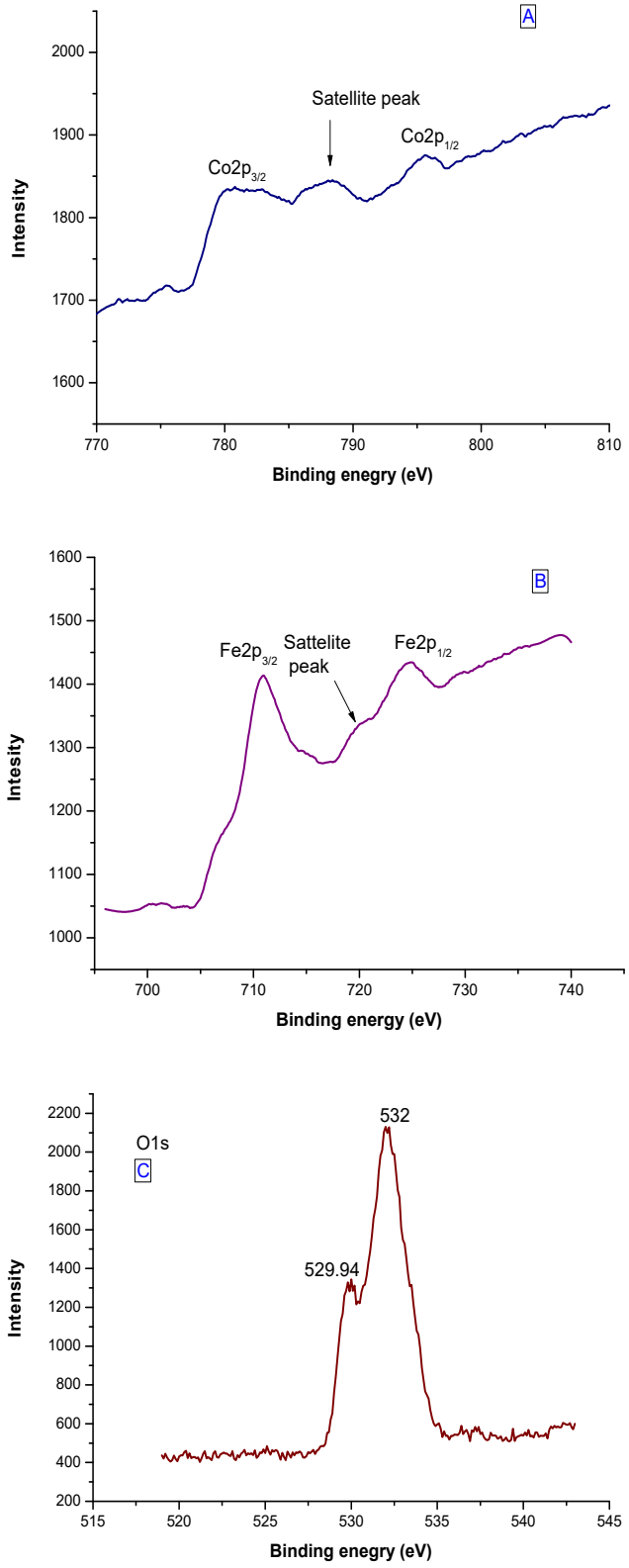

Fig 7: XPS of $CoFe_2O_4$ showing A) Co 2p, B) Fe 2p and C) O1s peaks

https://doi.org/10.15623/ijret.2018.0709004 Received: 16-06-2018, Accepted: 28-07-2018, Published: 18-08-2018

3.8 Photocatalytic Activity

Photocatalytic activity of $CoFe_2O_4$ was studied for the degradation of MO under the visible light illumination. Figure 8 represents the plot of C/C_o versus time. Where, C_o is the initial concentration and C is the concentration of substrate MO molecule at a given time't'. 250 ml of 10 ppm MO was degraded in a time period of 160 min with $CoFe_2O_4$ photocatalyst. The photocatalytic activity of $CoFe_2O_4$ was also studied in the presence of PMS which acts as an oxidant. The optimum concentration of PMS is found to be 10 ppm. The presence of PMS in a photocatalytic reaction is beneficial especially due to its unsymmetrical structure and dipolar nature of the molecule [21]. PMS has lower unoccupied molecular orbital (LUMO) energy levels which can readily accommodate the photogenerated electrons more efficiently and shows better oxidising reactions and the process may be termed as charge transfer to solvent molecule (CTTS) and PMS forms a charge transfer complex with $CoFe_2O_4$ which can always be expected when there are low lying unfilled orbital's in the solvent. These unfilled orbital's have strong affinity for electrons. The strength and stability of CTTS complex is in between the weak Vander Waals complexes and molecules bonded by strong valence forces [22-23]. The electron donating or accepting capability will also be different for ground state molecules and photoexcited state molecules. Co^{2+} ion in $CoFe_2O_4$ can easily bond with oxygen molecule by giving an electron. The resultant products can be Co^{3+} ion and super oxide radical. The peroxide ion in the PMS molecule $[-O-O]^{2-}$ has 18 electrons and the electronic configuration of the molecule can be represented in the following way:

$$\sigma 1s^2\ \sigma^* 1s^2\ \sigma 2s^2\ \sigma^* 2s^2\ \sigma 2p^2{}_x\ (\pi 2p^2{}_y, \pi 2p^2{}_z)(\pi^* 2p^2{}_y, \pi^* 2p^2{}_z)$$

The bond order is 1 and hence there should be a single bond between the two oxygens. Superoxide ion $[O_2]^{2-}$ has 17 electrons and has a similar electronic configuration like peroxide ion except π^*2p_z orbital has single electron and its bond order is 1.5. The peroxide and superoxide ions are larger in size, their stability increases in the solution based on the reaction conditions. Superoxide is a stronger oxidising agent than peroxide and they are capable of generating H_2O_2 and O_2 in presence of water or acids. This activated super oxide free radical can oxidise the organic substrate molecule. Simultaneously the reduction reaction involving super oxide radical can also lead to the formation of H_2O_2. The Fe^{3+} ion and Co^{2+} ions can also show photo-Fenton reactions in presence of In-situ generated H_2O_2. Classical photo-Fenton process (CPFP) involves ferrous ions and H_2O_2 in an homogeneous reaction system. H_2O_2 acts as an oxidant in the reaction. If other oxidants are used then, the process is referred to as modified photo-Fenton process (MPFP). In the present research PMS is used an oxidant instead of H_2O_2 and H_2O_2 is generated as a by product in the reaction. Therefore, both CPFP and MPFP reactions can occur simultaneously in the presence of PMS. Both oxidation and reduction mechanisms are beneficial for the photocatalytic degradation reaction. The oxidation states of transition metal ions like Co and Fe can vary and they can very easily exist in multiple oxidation states. Both these ions can occur in +2/+3 oxidation states based on the electron donating or electron accepting process. The back oxidation/reduction process can also occur under the conditions of illumination. The photogenerated electron trapped by either Fe^{3+} or by Co^{2+} ions changes its stable electronic configuration and the ions will spontaneously attain the stable state by either trapping/detrapping the electron during the photochemical reactions. Hence, these ions efficiently participate in the photocatalytic and photo-Fenton reaction process simultaneously (Eqs 1-4).

$$Co^{2+} + HSO_5^- \rightarrow Co^{3+} + SO_4^{\bullet -} + OH^- \quad (1)$$

$$Fe^{3+} + HSO^-_5 \rightarrow Fe^{2+} + SO_5^{\bullet -} + H^+ \quad (2)$$

$$Fe^{2+} + HSO^-_5 \rightarrow Fe^{3+} + SO_4^{\bullet -} + OH^- \quad (3)$$

$$HSO^-_5 \rightarrow SO_4^{\bullet -} + {}^{\bullet}OH \quad (4)$$

The various reaction process which are occurring can be listed as photocatalysis with $CoFe_2O_4$, CPFP with Co^{2+} / Fe^{3+} ions in presence of In-situ generated H_2O_2, MPFP with Co^{2+} / Fe^{3+} ions in presence of PMS and homolysis process of PMS may simultaneously occur and the synergistic effects between these reactions enhance the photocatalytic degradation rate and all these process are represented in the Figure 9. The CPFP reactions with either Fe^{2+} ions or advanced photo-Fenton process (APFP) where nano Fe^0 particles are used can only occur in the pH range of 2-3.5. This limitation is due to the process of corrosion of Fe^{2+} ions / Fe^0 nanoparticles since they form hydroxides at pH conditions above 3.5 and this limitation can be overcome by the use of $CoFe_2O_4$ [24]. In the present research, photo-Fenton reactions with $CoFe_2O_4$ can occur in the pH range of 6-7. The photolysis of PMS can result in hydroxyl and sulphate free radicals. But these free radicals in the absence of catalyst are short lived and are lost quickly and hence the degradation time period is observed to be 180 min. $CoFe_2O_4$ in presence of PMS shows an enhanced photocatalytic degradation rate and the enhancement is enormous which can be observed from the results presented in the Table 1. The various reactive species in the degradation process includes holes, bulk/surface hydroxyl free radicals, super oxide radicals etc.,. An effort is made to understand the mechanism of these photogenerated oxidising species which is essential in understanding the mechanism of photocatalysis. In this regard, methanol a hole scavenger was added to the photocatalytic degradation reaction. Holes are primary oxidising species in the photocatalytic reactions and they can be involved in the two reactions path ways: i) it can directly attack the surface adsorbed substrate molecules, ii) it reacts with surface adsorbed water or hydroxyl groups to produce oxidative hydroxyl free radicals which subsequently attacks the substrate molecules. In this process the lifetime of holes is in picoseconds time regime. The addition of methanol in the present reaction system demonstrated that the rate of degradation decreased

https://doi.org/10.15623/ijret.2018.0709004 Received: 16-06-2018, Accepted: 28-07-2018, Published: 18-08-2018

significantly. The excess hydroxyl free radicals which were generated due to the presence of PMS were completely quenched by the addition of methanol.

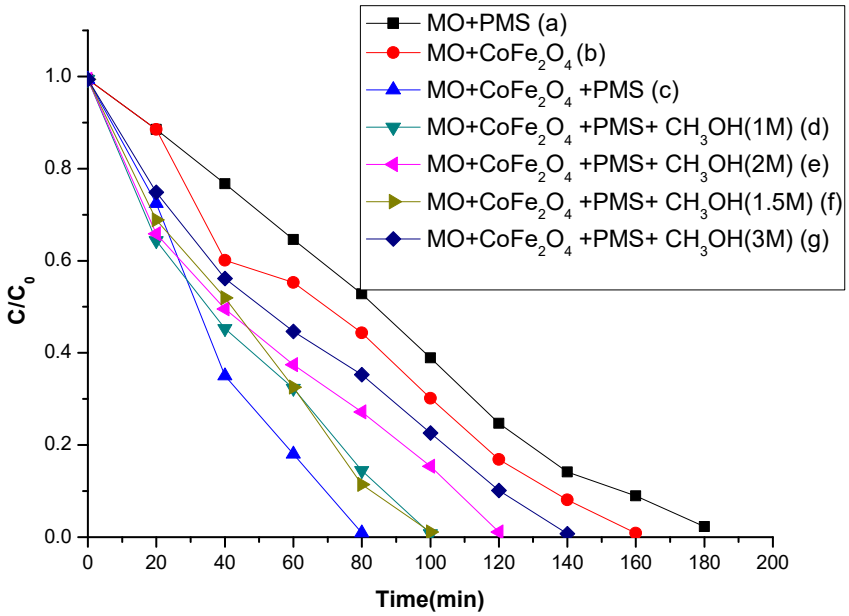

Fig 8: Plot of C/Co vs. time in minutes for the degradation of MO (10 ppm) along with (a) PMS, (b) $CoFe_2O_4$, (c) $CoFe_2O_4$/ PMS, (d) $CoFe_2O_4$/PMS/CH_3OH (1M),(e) $CoFe_2O_4$/PMS/CH_3OH (2M),(f) $CoFe_2O_4$/PMS/CH_3OH (1.5M), (g) $CoFe_2O_4$/PMS/CH_3OH (3M)

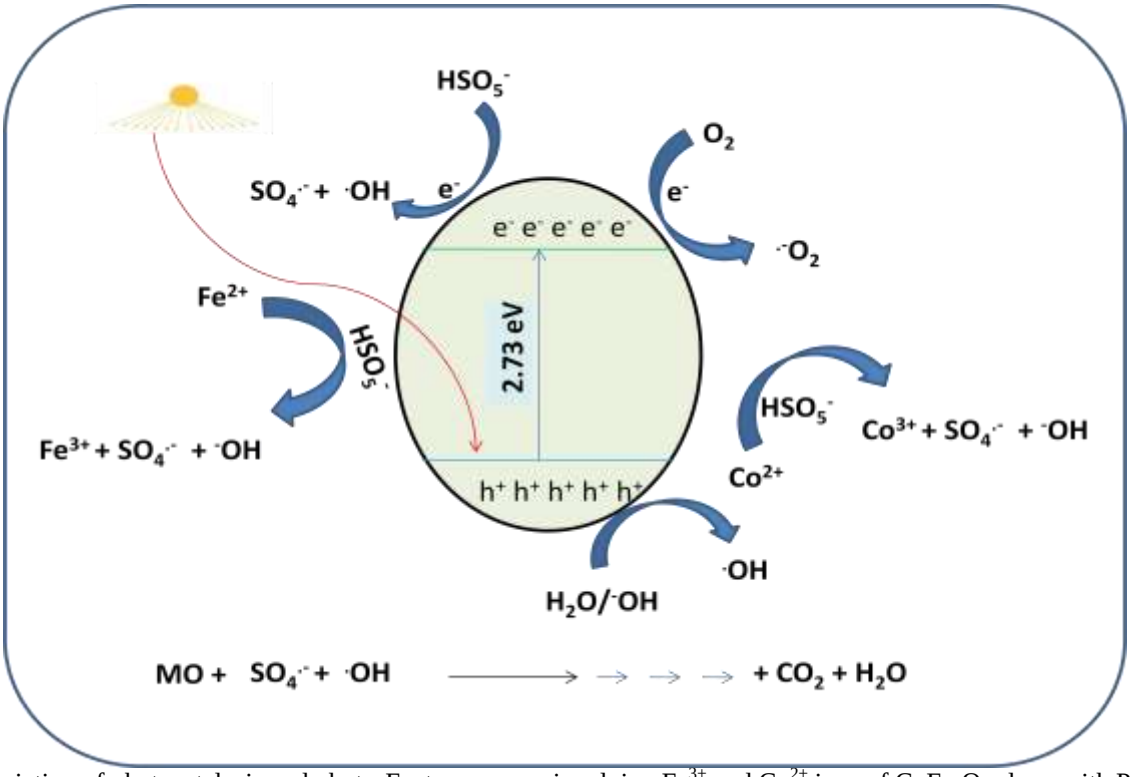

Fig 9: Depiction of photocatalysis and photo-Fenton process involving Fe^{3+} and Co^{2+} ions of $CoFe_2O_4$ along with PMS as an oxidant showing surface and bulk production of hydroxyl and sulphate free radicals under illumination of visible light.

https://doi.org/10.15623/ijret.2018.0709004 Received: 16-06-2018, Accepted: 28-07-2018, Published: 18-08-2018

3.9 Reusability of the Catalyst

To test the reusability of the catalyst, at the end of each experiment the $CoFe_2O_4$ catalyst particles were separated and then was washed thrice with distilled water. The percentage degradation decreases only nominally for the second cycle where as it decreased by 20% for the third consecutive cycle (Figure 10). Hence, the $CoFe_2O_4$ catalyst can be reused for at least two-three repetitive cycles.

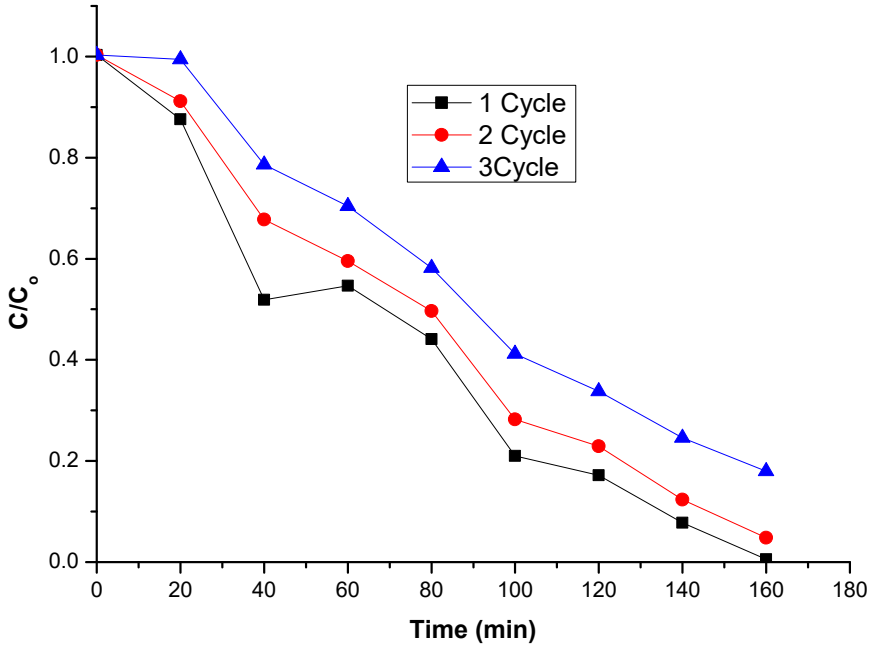

Fig 10: C/C_0 versus time plot to check the reusability of $CoFe_2O_4$ (100 mg) nanoparticles for three repeated consecutive cycles.

Table 1: Summarized experimental details for the degradation of MO at pH 6.2 (a)= 1st cycle, (b) = 2nd cycle and (c)= 3rd cycle

Sl NO.	Concentration MO (PPM)	Catalyst (mg)	PMS (PPM)	Scavenger Methanol (M)	Rate constant x 10^{-2} min^{-1}	Irradiation time
1	10	-	10	-	1.7728	180
2	10	100	-	-	2.7015	160
3	10	100	10	-	3.9332	80
4	10	100	10	1	3.1037	100
5	10	100	10	2	2.5471	120
6	10	100	10	1.5	3.2478	100
7	10	100	10	3	1.9821	140
8	10	100 (a)	-	-	2.3690	160
9	10	100 (b)	-	-	1.7255	160
10	10	100 (c)	-	-	1.0803	160

4. CONCLUSION

The presence of PMS in a photocatalytic reaction is beneficial especially due to its unsymmetrical structure, dipolar nature and tendency to generate super oxide radicals. PMS has low lying unoccupied molecular orbital's which can readily accommodate photogenerated electrons forming a CTTS complex. Photocatalysis with $CoFe_2O_4$, CPFP with Co^{2+} / Fe^{3+} ions in presence of In-situ generated H_2O_2, MPFP with Co^{2+} / Fe^{3+} ions in presence of PMS and homolysis process of PMS may simultaneously occur and the synergistic effects between these reactions enhance the photocatalytic degradation rate. Photo-Fenton reactions with $CoFe_2O_4$ can occur in the pH range of 6-7 which is otherwise not observed in the CPFP. Active role of hydroxyl free radicals in the degradation mechanism is confirmed by the addition of methanol to the reaction system.

https://doi.org/10.15623/ijret.2018.0709004 Received: 16-06-2018, Accepted: 28-07-2018, Published: 18-08-2018

ACKNOWLEDGEMENT

Author acknowledges the financial assistance from University Grants Commission (UGC) for DSA-SAP programme, Government of India.

REFERENCES

[1] N. Pinna, G. Neri, M. Antonietti, M. Niederberger, Nonaqueous, Nonaqueous synthesis of nanocrystalline semiconducting metal oxides for gas sensing, Angew. Chem. Int. Ed. 43 (2004) 4345–4349.

[2] O. Kuba, T.Ido , H Yokoyama, Engineering Electrical and Electronic Engineering. IEEE transactions on magnetic. 18 (1982) 1122-124.

[3] R Valenzuela, Magnetic Ceramics, Cambridge University Press, Cambridge, UK, 1994 1st edition.

[4] V. Hays, R. Marchand, G. Saindrenan and E.Garffet, Nanocrystalline Fe and Ni solid solutions prepared by mechanical alloying. Nanostructured Materials, (1996)7411-420.

[5] N. M. Deraz, Production and characterization of pure and doped copper ferrite nanoparticles. J. Analy. Appl Pyrls, 82 (2008) 212-222.

[6] H. Yang, J. Z. Lu , X. Cheng, Y. Tang, Photocatalytic activity evaluation of tetragonal CuFe2O4 nanoparticles for the H_2 evolution under visible light irradiation. J. Alloys compd, 476 (2009) 715-719.

[7] A. Kezzim, N. Nasrallah, A. Abdi, M. Trai, Visible light induced hydrogen on the novel hetero-system $CuFe_2O_4/TiO_2$. Energy conversion and Management, 52 (2011) 2800-2806.

[8] F.S. Li, L. Wang, J.B. Wang, Q.G. Zhou, X.Z. Zhou, H.P. Kunkel, G. Williams, Site preference of Fe in nanoparticles of $ZnFe_2O_4$. J. Magnetism and Mag.Mater. 268 (2004) 332-339.

[9] E. Manova, B. Kunev, D. Paneva, I. Mitov, L. Petrov, C. Estournes, C. D'Orleans, J.L. Rehspringer, M. Kurmoo, Mechano-Synthesis, Characterization, and Magnetic Properties of Nanoparticles of Cobalt Ferrite, $CoFe_2O_4$. J. Chem. Mater. 16 (2004) 5689.

[10] S. Joshi, V.B. Kamble, M. Kumar, A.M. Umarji, G. Srivastava, Nickel substitution induced effects on gas sensing properties of cobalt ferrite nanoparticles. J. Alloys Compd. 654 (2016) 460.

[11] B.G. Toksha, S.E. Shirsath, S.M. Patange, K.M. Jadhav, Structural investigations and magnetic properties of cobalt ferrite nanoparticles prepared by sol–gel auto combustion method. J. Solid State Commun. (2008) 147-479.

[12] S. Nilmoung, P. Kidkhunthod, S. Pinitsoontorn, S. Rujirawat, R. Yimnirun, S. Maensiri,. J. Mater. Sci. Proc. (2015)119-141.

[13] Ma, J. Graham, N.J.D, Degradation of atrazine by manganese-catalysed ozonation- influence of radical scavengers. Water Research 34, (2000) 3822-3828.

[14] Y. R. Smith, A. Kar, V. R. Subramanian, Investigation of physicochemical parameters that influence photocatalytic degradation of methyl orange over TiO_2 nanotubes, Ind. Eng. Chem. Res. 48 (2009)10268-10276.

[15] Y. M. Li, X. J Lv, J. Lu, J. Li, Preparation of SnO_2-nanocrystal/graphene-nanosheets composites and their lithium storage ability, J. Phys. Chem. C. 114, (2010) 21770−21774

[16] M. Fujihira, Y. Satoh, T. Osa, Heterogeneous photocatalytic oxidation of aromatic compounds on TiO2. Nature. 293 (1981)206−208.

[17] Noppakun Sanpo, Christopher C. Berndt, Cuie Wen, James Wang, Transition metal-substituted cobalt ferrite nanoparticles for biomedical applications. Acta Biomaterialia 9 (2013) 5830–5837

[18] R. Kavitha, L. Gomathi Devi, Synergistic effect between carbon dopant in titania lattice and surface carbonaceous species for enhancing the visible light photocatalysis, J. Environ. Chemi. Eng. 2 (2014) 857–867

[19] Z. W. Wang, D. Schiferl, Y. S. Zhao, S. C. O. Neill, High Pressure Raman Spectroscopy of Spinel-Type Ferrite $ZnFe_2O_4$, J. Phys. Chem. Solids. 64, (2003) 2517–2523.

[20] M. Maletin, E. G. Moshopoulou, A. G. Kontos, E Devlin, A. Delimitis, V. Zaspalis, L.Nalbandian, V. V. Srdic, Synthesis and Structural Characterization of In-Doped $ZnFe_2O_4$ Nanoparticles, J. Eur.Ceram. Soc. 27 (2007) 4391–4394.

[21] L. Gomathi Devi, M. Srinivas, Hydrothermal synthesis of reduced graphene oxide-$CoFe_2O_4$ heteroarchitecture for high visible light photocatalytic activity: Exploration of efficiency, stability and mechanistic pathways, J. Envi.Chem.Eng. 5 (2017) 3243-3255.

[22] K. K. Rohatgi – Mukherjee, Fundamentals of photochemistry, revised edition ,1986. Wiley Eastern limited.

[23] J. D. Lee, Concise Inorganic Chemistry, 5th edition 2007. John Wiley and sons

[24] L. Gomathi Devi, M. Srinivas, M.L. Aruna Kumari., 2016. Heterogeneous advanced photo-Fenton process using peroxymonosulfate and peroxydisulfate in presence of zero valent metallic iron: A comparative study with hydrogen peroxide photo-Fenton process, J. Water Process Eng. 13 (2016) 117–126.